G Model
CATTOD-10058; No. of Pages 9
ARTICLE IN PRESS
Catalysis Today xxx (2016) xxx–xxx

Contents lists available at ScienceDirect

Catalysis Today

journal homepage: www.elsevier.com/locate/cattod

# Structure/activity relationships applied to the hydrogenation of α,β-unsaturated carbonyls: The hydrogenation of 3-butyne-2-one over alumina-supported palladium catalysts

Clément G.A. Morisse [a], Alastair R. McInroy [a], Craig Anderson [a], Christopher J. Mitchell [b], Stewart F. Parker [c], David Lennon [a,*]

[a] School of Chemistry, Joseph Black Building, University of Glasgow, Glasgow G12 8QQ, UK
[b] Huntsman (Europe) BVBA, Everslaan 45, 3078 Everberg, Belgium
[c] ISIS Facility, STFC Rutherford Appleton Laboratory, Chilton, Didcot, Oxon OX11 0QX, UK

ARTICLE INFO

*Article history:*
Received 10 September 2015
Received in revised form 9 February 2016
Accepted 12 February 2016
Available online xxx

*Keywords:*
Heterogeneous catalysis
Alumina-supported palladium catalysts
3-Butyne-2-one hydrogenation
Structure/activity relationships

ABSTRACT

The gas phase hydrogenation of 3-butyne-2-one, an alkynic ketone, over two alumina-supported palladium catalysts is investigated using infrared spectroscopy in a batch reactor at 373 K. The mean particle size of the palladium crystallites of the two catalysts are comparable ($2.4 \pm 0.1$ nm). One catalyst ($Pd(NO_3)_2/Al_2O_3$) is prepared from a palladium(II) nitrate precursor, whereas the other catalyst ($PdCl_2/Al_2O_3$) is prepared using palladium(II) chloride as the Pd precursor compound. A three-stage sequential process is observed with the $Pd(NO_3)_2/Al_2O_3$ catalyst facilitating complete reduction all the way through to 2-butanol. However, hydrogenation stops at 2-butanone with the $PdCl_2/Al_2O_3$ catalyst. The inability of the $PdCl_2/Al_2O_3$ catalyst to reduce 2-butanone is attributed to the inaccessibility of edge sites on this catalyst, which are blocked by chlorine retention originating from the catalyst's preparative process. The reaction profiles observed for the hydrogenation of this alkynic ketone are consistent with the site-selective chemistry recently reported for the hydrogenation of crotonaldehyde, an alkenic aldehyde, over the same two catalysts. Thus, it is suggested that a previously postulated structure/activity relationship may be generic for the hydrogenation of α,β-unsaturated carbonyl compounds over supported Pd catalysts.



## 1. Introduction

A major goal in contemporary heterogeneous catalysis is to define structure/activity relationships for specified reactions [1,2]. Supported palladium catalysts have wide application in selective hydrogenation reactions [3], therefore it is highly desirable to correlate product yields with certain catalyst specifications, so that optimum catalyst formulations maximize the atom economies of particular unit operations. As an example of how the structure of Pd crystallites can be linked to product distributions, Kiwi-Minsker et al. have investigated the solution phase selective hydrogenation of alkynes over stabilized Pd nano-crystals and established the semi-hydrogenation of 2-methyl-3-butyne-2-ol to 2-methyl-3-butene-2-ol to be *structure sensitive* [4]. Further studies by this group involving supported Pd nano-particles concentrated on the well-studied gas phase hydrogenation of ethyne and demonstrated that the size and shape of the Pd nano-particle significantly affected the catalyst activity [5]. More recently, computational and experimental modeling have been employed to interrogate the structure sensitivity of 2-methyl-3-butyne-2-ol hydrogenation on Pd [6].

The present study considers how the morphology of Pd crystallites can influence selectivity branching in gas phase hydrogenation reactions of α,β-unsaturated carbonyl compounds. Studies by McInroy et al. examining the hydrogenation of crotonaldehyde over a series of alumina-supported Pd catalysts proposed a structure/activity correlation for hydrogenation of the α,β-unsaturated aldehyde [7]. Specifically, partial hydrogenation of crotonaldehyde to butanal was deemed to be *structure insensitive*, whereas the hydrogenation of butanal to butanol exhibited distinct *structure sensitivity* that was linked to the presence of a particular active site. Importantly, this site could be blocked in the catalyst preparation stage. Thus, the work demonstrated how an awareness of catalyst preparative procedures may be exploited to perturb product distributions [7].

* Corresponding author.
*E-mail address:* David.Lennon@glasgow.ac.uk (D. Lennon).

http://dx.doi.org/10.1016/j.cattod.2016.02.028

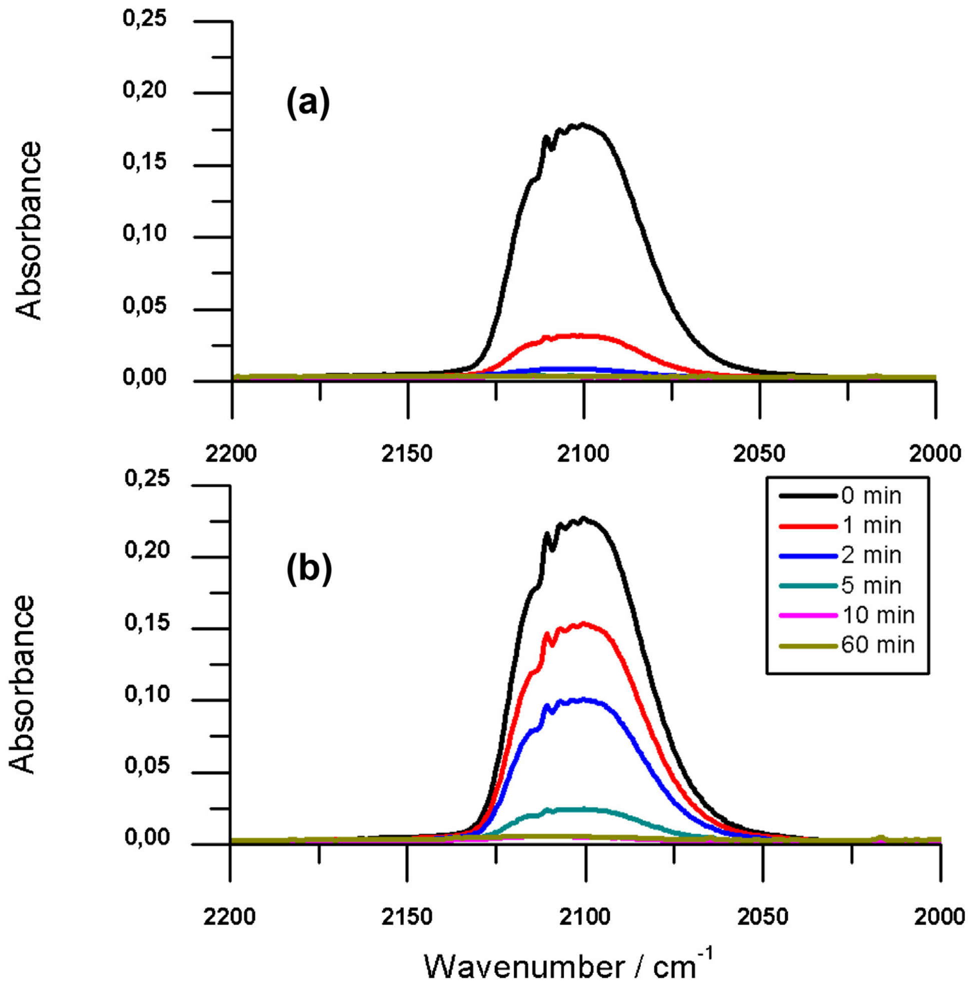


**Fig. 1.** The infrared spectrum (2200–2000 cm$^{-1}$) for the hydrogenation of 3-butyne-2-one as a function of time (0–60 min) over (a) $Pd(NO_3)_2/Al_2O_3$ and (b) $PdCl_2/Al_2O_3$.

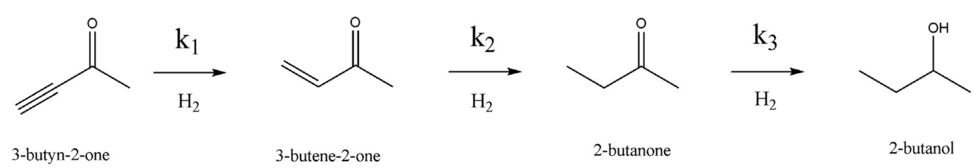


**Scheme 1.** A reaction scheme for the hydrogenation of 3-butyne-2-one. Stage 1 is the reduction of 3-butyne-2-one to produce 3-butene-2-one; Stage 2 is the reduction of 3-butene-2-one to produce 2-butanone; Stage 3 is the reduction of 2-butanone to produce 2-butanol. $k_1$–$k_3$ are the associated rate coefficients.

The nature of the active site attributed to enabling second stage hydrogenation activity within the crotonaldehyde hydrogenation system is ascribed to Pd (111)/(111) and (111)/(110) edge sites [7]. This hypothesis arises from an infrared spectroscopic investigation of the CO chemisorption properties of the same suite of alumina-supported palladium catalysts used in the crotonaldehyde study [8]. That work relied on an analysis of the infrared spectrum of carbon monoxide chemisorbed on a model high surface area alumina-supported palladium catalyst [9]. Further, temperature-programmed desorption studies of isotopically substituted CO on two of the $Pd/Al_2O_3$ catalysts [10] also contributed to an awareness of the morphological traits of these catalysts.

As a consequence of Pd's inherent preference for hydrogenating C=C bonds in preference to C=O bonds [11], the hydrogenation of α,β-unsaturated carbonyl compounds is infrequently studied over supported Pd catalysts. However, notable studies by Ide and co-workers have examined the effectiveness of supported metal catalysts for the hydrogenation of unsaturated ketones (methyl vinyl ketone and benzalacetone) and unsaturated aldehydes (crotonaldehyde and cinnamaldehyde) [12]. Despite favourable turnover frequencies, a Pd/C catalyst preferentially hydrogenated the C=C bond rather than the C=O bond, with supported Pt, Ru and Au catalysts exhibiting higher selectivity for the desired unsaturated alcohol [12]. Rather than concentrating on the selective formation of unsaturated alcohols from α,β-unsaturated carbonyl compounds, the work of McInroy et al. used the partial and complete hydrogenation pathways accessible in the $Pd/Al_2O_3$/crotonaldehyde/$H_2$ reaction system to distinguish site specificity for partial and complete hydrogenation reactions [7]. Presently, that correlation has only been explored for the hydrogenation of crotonaldehyde, an α,β-unsaturated aldehyde.

The present work seeks to discover if the proposed structure/activity relationship can be extended to α,β-unsaturated ketones. This will then provide insight on the possible generic nature of the postulated site-selective model for hydrogenation reactions over supported Pd catalysts. Thus, the hydrogenation

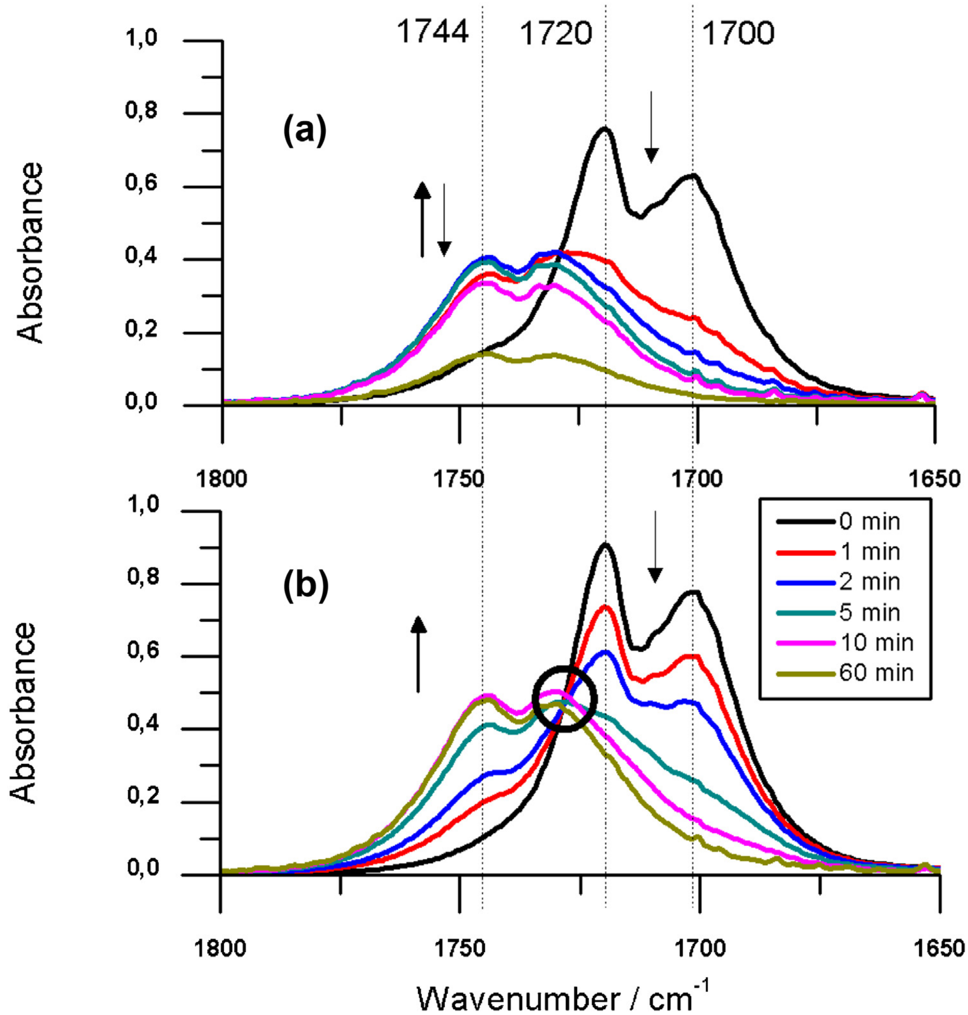


**Fig. 2.** The infrared spectrum (1800–1650 $cm^{-1}$) for the hydrogenation of 3-butyne-2-one as a function of time (0–60 min) over (a) $Pd(NO_3)_2/Al_2O_3$ and (b) $PdCl_2/Al_2O_3$. The arrows signify the intensity trend as a function of time for bands at 1744 and 1700 $cm^{-1}$. The circle in (b) signifies an isosbestic point at 1730 $cm^{-1}$.

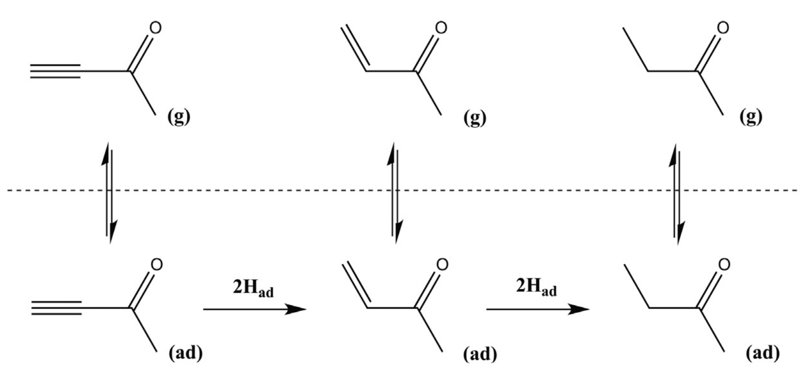


**Scheme 2.** Equilibria contributing to the isosbestic point at 1730 $cm^{-1}$ associated with the $PdCl_2/Al_2O_3$ catalyst, Fig. 2(b). The (g) and (ad) subscripts designate respectively gaseous and adsorbed phases of the reacting molecules.

**Table 1**
A summary of catalyst characterisation details [8]. The two samples were examined for C, H, N and Cl by elemental analysis, with only positive values included in the table. CO chemisorption saturation values were performed at 293 K. The errors represent one standard deviation determined from a number of replicate experiments. Mean particle size is calculated from the CO chemisorption values according to assumptions described in reference [8].

| Source of Pd in catalyst | Pd loading (wt%) | BET ($m^2\,g^{-1}$) | Elemental analysis (wt.%) | Saturation coverage of CO ($\mu$mol CO $g_{(cat)}^{-1}$) | Catalyst dispersion (%) | Calculated Pd mean particle size (nm) |
|---|---|---|---|---|---|---|
| $Pd(NO_3)_2$ | 4.0 | 102.6 | 0.8% N | 90.9 ± 15 | 48 ± 8 | 2.3 |
| $PdCl_2$ | 0.91 | 70.9 | 5.4% Cl | 19.5 ± 1.4 | 46 ± 3 | 2.5 |

Please cite this article in press as: C.G.A. Morisse, et al., Structure/activity relationships applied to the hydrogenation of α,β-unsaturated carbonyls: The hydrogenation of 3-butyne-2-one over alumina-supported palladium catalysts, Catal. Today (2016), http://dx.doi.org/10.1016/j.cattod.2016.02.028

G Model
CATTOD-10058; No. of Pages 9
ARTICLE IN PRESS



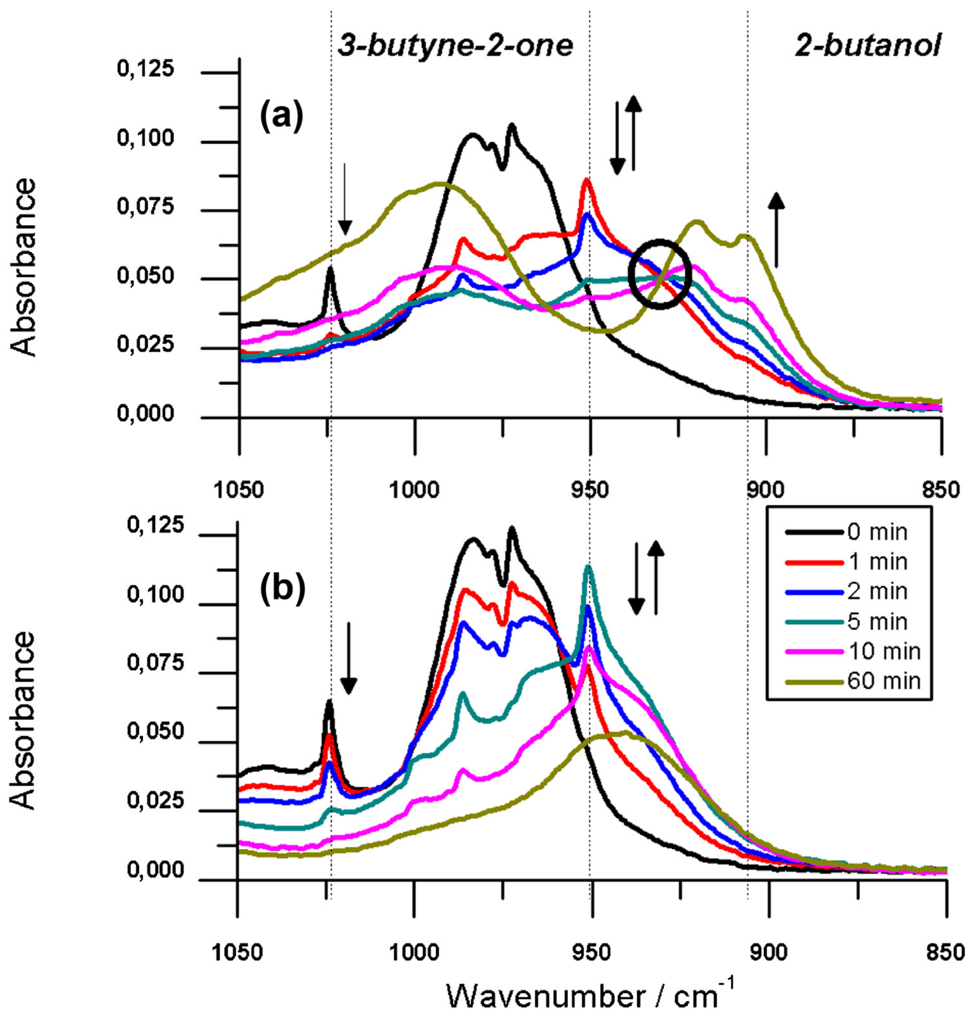


**Fig. 3.** The infrared spectrum (1050–850 cm$^{-1}$) for the hydrogenation of 3-butyne-2-one as a function of time (0–60 min) over (a) $Pd(NO_3)_2/Al_2O_3$ and (b) $PdCl_2/Al_2O_3$. The arrows signify the intensity trend as a function of time for bands at 1025, 950 and 900 cm$^{-1}$. The circle in (a) signifies an isosbestic point at 928 cm$^{-1}$.

of an alkynic ketone is studied over two $Pd/Al_2O_3$ catalysts considered in the original crotonaldehyde study [7]. One catalyst ($Pd(NO_3)_2/Al_2O_3$) is prepared from a palladium(II) nitrate precursor, whereas the other catalyst ($PdCl_2/Al_2O_3$) is prepared using palladium(II) chloride as the Pd precursor compound. Table 1 lists the physical characteristics of the two catalysts [8].

The catalysts were selected because, despite possessing comparable Pd particle sizes (2.4 ± 0.1 nm, Table 1), they exhibit highly distinct reaction profiles for crotonaldehyde hydrogenation. Specifically, $Pd(NO_3)_2/Al_2O_3$ facilitates crotonaldehyde and butanal hydrogenation to produce butanol, however, hydrogenation activity terminates at butanal with $PdCl_2/Al_2O_3$ [7]. The inability of the $PdCl_2/Al_2O_3$ catalyst to permit reduction of the carbonyl group is attributed to chloride residues present at the catalyst surface [7]. Whereas it is conceded that the high chloride residue evident in Table 1 relates to the catalyst pre-activation, infrared measurements of CO chemisorption after a catalyst reduction treatment establish chloride to remain present at the metal surface after a reduction stage [8]. Consequently, it is the blocking of specific Pd crystallite sites by residual chloride originating from the catalyst preparative stage that is thought to be influencing the crotonaldehyde reaction profiles over these two catalysts [7].

In the present work, the hydrogenation of 3-butyne-2-one ($CH{\equiv}C(C{=}O)CH_3$) in the gas phase is examined over samples of the two catalysts described above: $Pd(NO_3)_2/Al_2O_3$ and $PdCl_2/Al_2O_3$. Scheme 1 demonstrates the three sequential hydrogenation pathways accessible with this reaction system. Firstly, the alkyne ketone can be reduced to an alkene ketone (3-butene-2-one), which may be subsequently reduced to a saturated ketone (2-butanone) and, finally, the 2-butanone may be further reduced to a secondary alcohol (2-butanol).

This consideration of 3-butyne-2-one as a reactant provides the opportunity to examine the reduction of *sp*-hybridised carbon atoms as well as the *sp*$^2$-hybridised carbon atoms encountered in crotonaldehyde; whilst additionally permitting an examination of a ketone compared to an aldehyde. Given the variety of functional transformations evident within Scheme 1, infrared analysis of the mixture within a batch reactor is selected to examine the reaction chemistry. Periodic scanning of the gas phase enables the change in the gaseous phase present over the catalyst to be determined as a function of time [13–15]. In certain circumstances, the infrared spectrum can additionally provide information on conformational options attainable for the reagents and products throughout the full reaction coordinate [16], although that prospect is not considered in detail in this work. The benefits and disadvantages of the use of infrared spectroscopy within a catalytic batch reactor are considered elsewhere [15]. The present study makes extensive use of a recently published vibrational analysis of the four $C_4$ molecules indicated in Scheme 1 [17].

The work shows that the structure/activity relationship originally proposed for crotonaldehyde hydrogenation [7] is equally applicable to the hydrogenation of an alkynic ketone, implying that

Please cite this article in press as: C.G.A. Morisse, et al., Structure/activity relationships applied to the hydrogenation of α,β-unsaturated carbonyls: The hydrogenation of 3-butyne-2-one over alumina-supported palladium catalysts, Catal. Today (2016), http://dx.doi.org/10.1016/j.cattod.2016.02.028

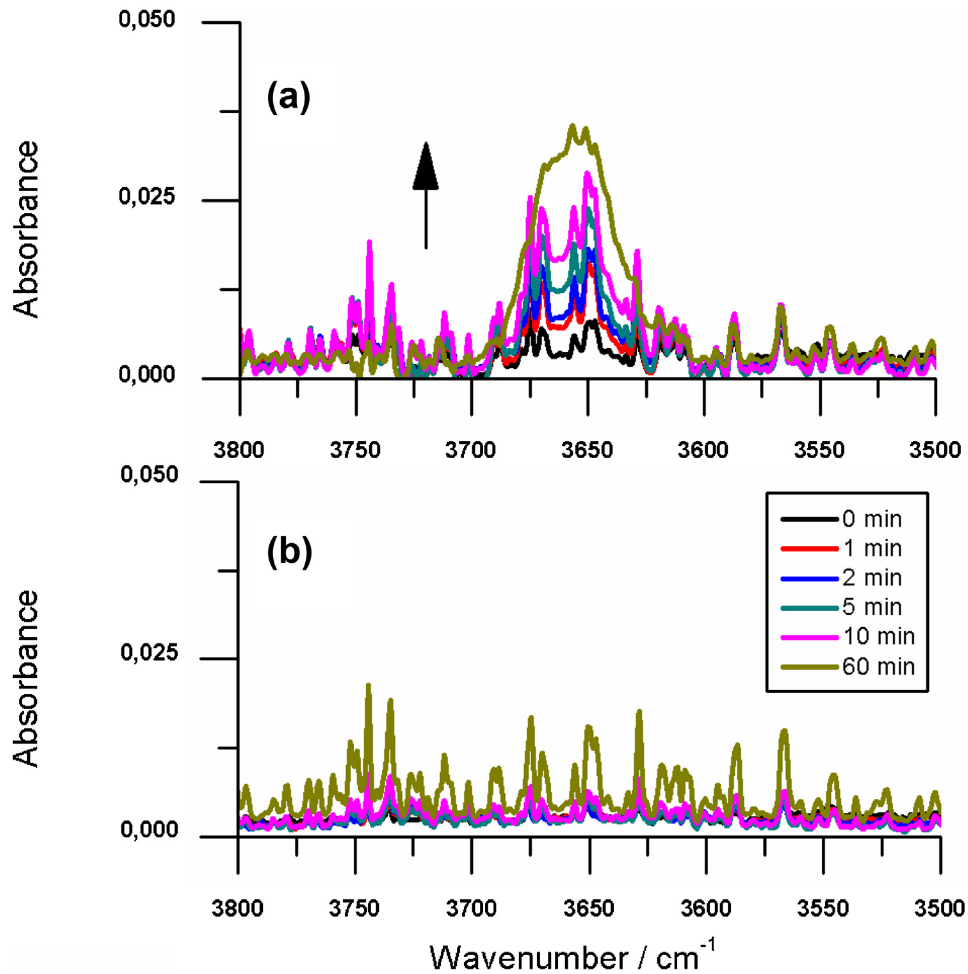


**Fig. 4.** The infrared spectrum (3800–3500 $cm^{-1}$) for the hydrogenation of 3-butyne-2-one as a function of time (0–60 min) over (a) $Pd(NO_3)_2/Al_2O_3$ and (b) $PdCl_2/Al_2O_3$. The arrow signifies the intensity trend as a function of time for the band at 3655 $cm^{-1}$.

the site-selective model is generic for the hydrogenation of α,β-unsaturated carbonyls over supported Pd catalysts. The implication of this outcome for evaluating morphological traits of supported Pd catalysts is briefly explored. A heightened awareness of metal crystallite morphological contributions to product distributions should lead to more efficient catalysis.

## 2. Experimental

Information on the preparation and characterization of the $Pd(NO_3)_2/Al_2O_3$ and $PdCl_2/Al_2O_3$ catalysts is presented elsewhere [8]. Reaction testing used a modified Graseby-Specac 5660 heated gas cell fitted with KBr windows and a 20140 automatic temperature controller. An injection septum within the cell enabled 3-butyne-2-one (Aldrich, 99% purity) to be added to the reaction system. The tubular cell had no facility for further mixing or re-circulation of gases. Two Brooks 5850E mass flow devices controlled the flow of hydrogen (BOC, 99.995% purity) and helium (BOC, CP grade 99.999% purity) *via* an in-line purifier (Messer Grieshiem Oxisorb) into a 50 $cm^3$ stainless steel mixing vessel that was packed with glass beads before entering into the reaction cell. A back-pressure regulator plus pressure gauge (Norgen) and shut-off valves allowed the cell to be isolated and the pressure monitored. The reactor was housed within a Nicolet Avatar 360 FTIR spectrometer equipped with a deuterated triglycine sulphate detector. The reactor is connected to the spectrometer internal gas purge facility *via* rubber sleeves. The spectrometer is continually purged with dry air, from which the $CO_2$ component has been removed (Donaldson Ultrafilter). These arrangements minimise atmospheric contributions to the infrared spectrum.

The catalyst was loaded into the reactor as a pressed disc. The catalyst was mounted within a glass sample holder that locates within the base of the cell, so that the catalyst was not in the path of the infrared beam. In this way, all spectra presented arise from the composition of the gaseous phase, with no contribution from the catalyst or the catalyst surface. The rate of 3-butyne-2-one hydrogenation was directly proportional to the mass of catalyst used, consistent with the reaction being under kinetic control and possessing no mass transport restrictions.

The catalyst mass, quantity of hydrocarbon and pressure of hydrogen were selected to yield a full hydrogenation profile within *ca.* 1 h, so that infrared spectra of sufficient signal/noise ratio could be repeatedly recorded during that interval. In this manner, *ca.* 20 mg of the catalyst was pressed into a thin disc using a 13 mm die (Specac) pressurised at 12 t by a hydraulic press (PerkinElmer). The catalyst disc was reduced in the following manner: The cell temperature was maintained at 303 K and a mixture of 10% $H_2$/90% He was passed through the reactor at a flow rate of 20 ml $min^{-1}$ for 30 min. The hydrogen composition was increased to yield an equimolar mixture of hydrogen and helium at the same flow rate and the temperature was increased to 373 K then maintained at that temperature. After 30 min under these conditions, the reactor was isolated at a pressure of 900 Torr (0.12 MPa). A liquid chromatography syringe (Hamilton Bonaduz) was used to inject a 5.0 μl aliquot

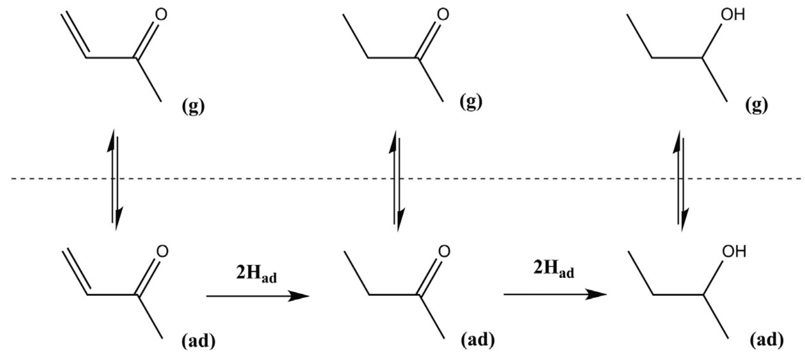


**Scheme 3.** Equilibria contributing to the isosbestic point at 928 $cm^{-1}$ associated with the $Pd(NO_3)_2/Al_2O_3$ catalyst, Fig. 2(b). The (g) and (ad) subscripts designate respectively gaseous and adsorbed phases of the reacting molecules.

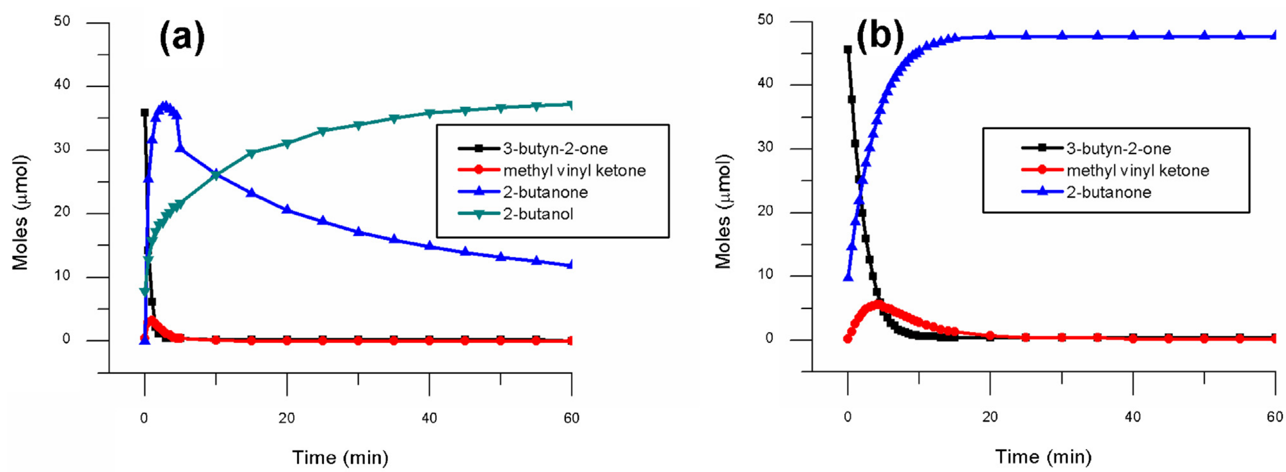


**Fig. 5.** (a) Reaction profile for the hydrogenation of 3-butyne-2-one as a function of time over $Pd(NO_3)_2/Al_2O_3$. (b) Reaction profile for the hydrogenation of 3-butyne-2-one as a function of time over $PdCl_2/Al_2O_3$.

of 3-butyne-2-one into the cell *via* the septum. The 3-butyne-2-one was used without further purification. Scanning of the infrared spectrum commenced as soon as the injection of the 3-butyne-2-one was complete. This combination of reagents results in a hydrogen:hydrocarbon ratio of 44:1 and a hydrocarbon:Pd(s) ratio of 82:1 for the $PdCl_2$ catalyst, *i.e.* hydrogen is in excess of the hydrocarbon and the hydrocarbon is in excess of palladium surface atoms. Thus, the infrared cell is acting as a batch reactor under conditions where reasonable conversions represent multiple turnovers, unhindered by the availability of hydrogen. Infrared spectra were recorded at a resolution of 4 $cm^{-1}$, co-adding 8 scans and requiring an acquisition time of *ca.* 10 s. The reaction temperature was maintained at 373 K and ensured that all the reagents remained in the gaseous phase. Measurements were performed in triplicate, with representative datasets being presented here. Hydrogenation experiments on an alumina disc (no Pd) that had been treated in the same manner as outlined above showed no conversion of 3-butyne-2-one, establishing the hydrogenation reactions to be metal-mediated.

The Beer-Lambert law is applicable under the designated reaction conditions, permitting calibration curves to be readily produced. As-received samples of 3-butene-2-one (Aldrich, 99% purity), 2-butanone (Aldrich, 99.5% purity) and 2-butanol (Aldrich, 99.5% purity) were used as calibrants.

Mode assignments were made using density functional theory and validated by comparison of the calculated spectra to reference infrared and inelastic neutron scattering spectra. This work is comprehensively described in reference [17].

## 3. Results and discussion

The infrared spectra for reactions involving the two catalysts are presented in four spectral regions that emphasize the dynamics of specific functional entities. This intensity data is then used to determine the reaction profile for the 3-butyne-2-one hydrogenation process over each catalyst. Differences in the product distribution as a function of time are discussed in terms of the range of sites present on the Pd crystallites.

### *3.1. 2200–2000 $cm^{-1}$*

Fig. 1 presents the infrared spectra in the $\nu$(C≡C) region of the spectrum (2200–2000 $cm^{-1}$) as a function of time. The broad peak at t = 0 centered at 2103 $cm^{-1}$ is the C≡C stretch of 3-butyne-2-one [17,18,19(a),20(a)]. The intensity of this feature for the $Pd(NO_3)_2/Al_2O_3$ catalyst (Fig. 1(a)) decreases rapidly on increasing reaction time, so that within *ca.* 2 min the band is no longer observable. This profile indicates a rapid hydrogenation of the alkyne C≡C bond; corresponding to a reaction turnover frequency of $3.21 \times 10^{17}$ 3-butyne-2-one molecules $s^{-1}$ and a turnover number of 18 3-butyne-2-one molecules $Pd_{(s)}{}^{-1}$. Fig. 1(b) shows the process to be significantly slower for the $PdCl_2/Al_2O_3$ catalyst, with complete reduction of the C≡C bond requiring *ca.* 10 min; corresponding to a reaction turnover frequency of $6.42 \times 10^{16}$ 3-butyne-2-one molecules $s^{-1}$ and a turnover number of 82 3-butyne-2-one molecules $Pd_{(s)}{}^{-1}$.

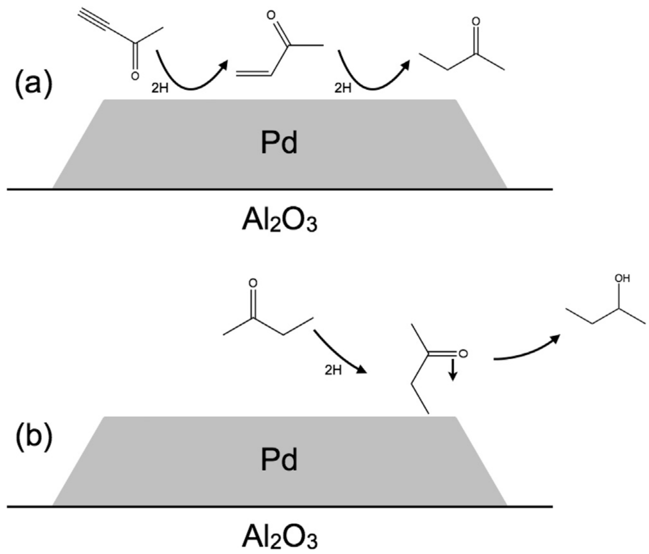


**Fig. 6.** Schematic representation (side view) of the site-selective nature of the hydrogenation of 3-butyne-2-one over supported Pd catalysts. (a) Pd crystallite where 3-butyne-2-one molecules are firstly hydrogenated to 3-butene-2-one and then, secondly, to 2-butanone over non-specific Pd sites. (b) Pd crystallite where the carbonyl group of 2-butanone is aligned with the edge sites of the crystallite; this adsorption geometry facilitates the hydrogenation of 2-butanone to form 2-butanol.

### 3.2. 1800–1650 $cm^{-1}$

Fig. 2 presents the infrared spectra in the ν(C═O) region of the spectrum (1800–1650 $cm^{-1}$) as a function of time. At t = 0, two bands at 1722 and 1702 $cm^{-1}$ are observed which correspond to the P and R branches of the C═O stretching mode of 3-butyne-2-one [17,18,19(a),20(a)]. Upon reaction, in the case of the $Pd(NO_3)_2/Al_2O_3$ catalyst (Fig. 2(a)), band intensity at 1722 and 1702 $cm^{-1}$ decreases and two higher wavenumber features are seen at 1744 and 1730 $cm^{-1}$. The intensity profile of the new doublet is best illustrated by the band at 1744 $cm^{-1}$, which is further removed from contributions from the 1720 $cm^{-1}$ band. After 1 min, the intensity of the 1744 $cm^{-1}$ band increases, maximizes at 5 min, then progressively decreases. The 1744/1730 $cm^{-1}$ doublet, now signifying ν(C═O) of an aliphatic ketone [17,21,19(b),20(b)] is still present after 60 min reaction time.

The sequence of changes in band intensities is more clearly seen in the case of the $PdCl_2/Al_2O_3$ catalyst, Fig. 2(b). Upon reaction, there is a more gradual decrease in intensity of the 1722 and 1702 $cm^{-1}$ peaks, that is concomitantly accompanied by the appearance of bands at 1744 and 1730 $cm^{-1}$ that represent 2-butanone [17,21,19(b),20(b)]. In contrast to the profile seen in Fig. 2(a), the intensity of the 1744 $cm^{-1}$ peak is seen to gradually increase up to a maximum value at 10 min that remains unchanged up to 60 min reaction time. Fig. 2(b) is additionally characterized by an isosbestic point at 1730 $cm^{-1}$, as the conjugated carbonyl grouping is transformed in to an aliphatic carbonyl.

Comparing the trends evident in Fig. 2, ν(C═O) shifts to higher wavenumber as *sp*- and *sp*$^2$-hybridised carbon atoms are reduced to *sp*$^3$-hybridised carbon atoms [17,19(c)]. Thus, the $Pd(NO_3)_2/Al_2O_3$ catalyst supports reduction of 3-butyne-2-one to 3-butene-2-one, which is then reduced to the aliphatic ketone (2-butanone), that is itself partially consumed within a reaction time of 60 min. However, in the case of the $PdCl_2/Al_2O_3$ catalyst (Fig. 2b), Stage 3 chemistry (2-butanone → 2-butanol) is not possible under these reaction conditions. No deviation from the chemistry outlined in Scheme 1 is apparent in this series of spectra.

It is noted that all of the spectra in Fig. 2(b), including t = 0, connect to the isosbestic point at 1730 $cm^{-1}$. The presence of this

**Table 2**
Vibrational modes selected to signify the quantity of reagent/products present in the reactor as a function of reaction time.

| Molecule | Mode | Wavenumber ($cm^{-1}$) |
|---|---|---|
| 3-Butyne-2-one | ν(C≡C) | 2103 |
| 3-Butene-2-one | ρ(═$CH_2$) | 950 |
| 2-Butanone | ν(C═O) | 1744 |
| 2-Butanol | ρ($CH_3$) | 905 |

feature hints at 3-butyne-2-one, 3-butene-2-one and 2-butanone being in equilibrium over the $PdCl_2/Al_2O_3$ catalyst. Cohen and Fischer have established the conditions under which isosbestic points are observed in the spectra of multi-component systems [22]. For a closed system, it is necessary that (i) the spectra of the limiting species intersect and (ii) that changes in the concentrations of the various species are linearly related. Consecutive reactions are not expected to yield isosbestic points [23]. Further, Croce has examined the case of competing reaction mechanisms involving several absorbing species, as is the case here, and establishes that a consecutive reaction mechanism will not exhibit isosbestic points [23]. A recent illustration of this position is outlined by Pojarlieff and co-workers who have examined different pathways connected with the acid catalysed intra-molecular attack of the β-phenylthiourea group of an amide function [24].

The fact that an isosbestic point is readily discernible at 1730 $cm^{-1}$ is therefore interpreted as demonstrating a greater degree of sophistication in the interactions between the reacting species than that defined by Scheme 1. One possibility could be the presence of a competing parallel reaction not described within Scheme 1. In particular, if hydrogenation of the carbonyl is competitive with alkyne and alkene hydrogenation then the presence of 3-butyne-2-ol and 3-butene-2-ol would be expected. For the $PdCl_2/Al_2O_3$ catalyst this pathway can be definitively eliminated because there is no evidence for alcohol formation in the O—H stretch region (see Section 3.4). For the $Pd(NO_3)_2/Al_2O_3$ catalyst, the presence of 2-butanol means that the O—H stretch is not definitive because the O—H stretch of all three alcohols occurs within a few wavenumbers of each other. However, 3-butyne-2-ol has characteristic modes at 805 and 925 $cm^{-1}$ for which there is no evidence in the spectra, in particular, the former occurs in a region where there are no modes from the other species providing confidence in this assertion. It is more difficult to be certain that 3-butene-2-ol is not present as all of its modes occur in regions where the other species contribute. Nonetheless, its strongest modes occur at 932 and 1056 $cm^{-1}$ and there are no distinct peaks at these positions. Thus, while we cannot definitively eliminate the possibility that 3-butene-2-ol is present in the case of the $Pd(NO_3)_2$-based catalyst, the similarity of the spectra of both catalysts in the early stages of the reaction sequence would strongly argue that it is not present over either catalyst.

Rather, the appearance of an isosbestic point is thought to reflect the role of adsorbed species in the transformations indicated in Scheme 1. Scheme 2 presents the specific interactions thought to be connected with the appearance of the 1730 $cm^{-1}$ isosbestic point in Fig. 2(b). Namely, an exchange of reagents/products at the gas/solid interface that, simultaneously, co-exist with surface-mediated hydrogenation reactions. Although the reaction sequence as observed may still be classed as a three stage consecutive process as outlined in Scheme 1 (A → B → C → D), the infrared based methodology utilized here is indicating further subtlety within the global process. Thus, Scheme 2 is proposed as a more comprehensive description of the elementary processes active within the reaction system. Being able to obtain such information on the equilibria active over the catalyst during multi-stage transformations is one of the advantages in using an IR cell as a batch reactor [15].

Please cite this article in press as: C.G.A. Morisse, et al., Structure/activity relationships applied to the hydrogenation of α,β-unsaturated carbonyls: The hydrogenation of 3-butyne-2-one over alumina-supported palladium catalysts, Catal. Today (2016), http://dx.doi.org/10.1016/j.cattod.2016.02.028

### 3.3. 1050–850 $cm^{-1}$

The temporal dependence of the infrared spectra in the range 1050–850 $cm^{-1}$ as a function of time is presented in Fig. 3 and contains information on acetylenic modes as well as olefinic wags. At t = 0 the spectrum is characterized by a low intensity sharp peak at 1024 $cm^{-1}$ and a broad peak centered around 980 $cm^{-1}$. These two bands are assigned to methyl rocking modes of 3-butyne-2-one [17]. Concentrating first on the spectrum connected with the $Pd(NO_3)_2/Al_2O_3$ catalyst (Fig. 3(a)), both of the fore-mentioned bands decrease dramatically within 1 min, signifying the loss of the alkynic unit. At 1 min a new band appears at 950 $cm^{-1}$, which then subsequently decreases in intensity on increasing time and is no longer discernible after 10 min. This is assigned to the vinyl rock of the *s-trans* conformer of 3-butene-2-one [17]. From 10 min onwards a doublet with peaks at 920 and 905 $cm^{-1}$ and a broad peak at 990 $cm^{-1}$ become apparent and increase in intensity up to 60 min. These features are assigned to methyl rocking modes of 2-butanol [17] and signify reduction of the 3-butyne-2-one all the way through to the secondary alcohol.

With the exception of the t = 0 spectrum, all of the spectra in Fig. 3(a) contribute to the isosbestic point at 928 $cm^{-1}$. This coincidence of bands is therefore thought to reflect interactions between 3-butene-2-one, 2-butanone and 2-butanol over the $Pd(NO_3)_2/Al_2O_3$ catalyst. Scheme 3 presents the adsorption/desorption stages thought to be responsible for the observed isosbestic point.

Fig. 3(b) presents the spectrum for the reaction catalysed by $PdCl_2/Al_2O_3$. The decrease of intensity of the 3-butyne-2-one methyl rocking modes at 1024 and 980 $cm^{-1}$ as a function of time are slower than that observed for $Pd(NO_3)_2/Al_2O_3$, following the trend seen in Fig. 1 for the $\nu$(C≡C) mode. The methyl rocking mode of 3-butene-2-one at 950 $cm^{-1}$ is apparent at 1 min, increases in intensity up to 5 min, and then decreases thereafter. The methyl rocking modes of 2-butanol seen in Fig. 3(a) with band maxima at 990, 920 and 905 $cm^{-1}$ are absent; in a consistent manner to the trend observed for the plateau of intensity of the $\nu$(C=O) mode of 2-butanone seen at 1744 $cm^{-1}$ in Fig. 2(b).

Thus, Fig. 3 strengthens the case that 3-butyne-2-one hydrogenation is faster over the $Pd(NO_3)_2/Al_2O_3$ catalyst and that, under the test conditions studied here, 2-butanol formation is not possible over the $PdCl_2/Al_2O_3$ catalyst.

### 3.4. 3800–3500 $cm^{-1}$

The vibrational spectrum about the (O—H) stretching region is shown in Fig. 4. From 1 min onwards the spectrum for the $Pd(NO_3)_2/Al_2O_3$ catalysed reaction, Fig. 4(a), shows increasing growth of a band centered at 3655 $cm^{-1}$, that is readily assigned to the $\nu$(O—H) of 2-butanol [17]. This feature is absent in the $PdCl_2/Al_2O_3$ set of spectra, Fig. 4(b), confirming 2-butanone reduction not to be possible over this catalyst under these conditions.

### 3.5. Reaction profiles

The following bands were selected to represent the four components of Scheme 1: 3-butyne-2-one, the C≡C stretch at 2103 $cm^{-1}$; 3-butene-2-one, the =$CH_2$ rock at 950 $cm^{-1}$; 2-butanone the C=O stretch at 1744 $cm^{-1}$; and 2-butanol, the methyl rock at 905 $cm^{-1}$, Table 2. Calibration of these spectral features by reference compounds enabled the extinction coefficients for these modes in the designated reaction conditions to be determined, so that concentration profiles could be produced. The resulting reaction profiles for the $Pd(NO_3)_2/Al_2O_3$ and $PdCl_2/Al_2O_3$ catalysts are presented in Fig. 5.

Fig. 5(a) presents the reaction profile for the $Pd(NO_3)_2/Al_2O_3$ catalyst, that is entirely consistent with a three-stage consecutive reaction. Firstly, 3-butyne-2-one is fully hydrogenated within 2.5 min. This rapid decrease of starting material is accompanied by the temporary presence of 3-butene-2-one, which attains maximum intensity at 1 min and, thereafter, progressively decreases in intensity up to 5 min, when this intermediate species is fully consumed. Throughout this period there is a proportionally greater increase in 2-butanone production, which achieves maximum intensity at 4 min then progressively decreases in intensity on continued reaction time. 2-Butanol production is detected at the onset and presents a growth profile throughout the full reaction coordinate, being the dominant molecular species at 60 min reaction time. With reference to Scheme 1, it is apparent from Fig. 5 that the magnitudes of the rate coefficients adopt the following order:

$$k_1 >> k_2 > k_3 \tag{1}$$

The reaction profile of the $PdCl_2/Al_2O_3$ catalyst is presented in Fig. 5(b) and is noticeably different to that seen for the $Pd(NO_3)_2/Al_2O_3$ catalyst. 3-Butyne-2-one consumption is much more gradual, requiring in excess of 10 min for complete conversion. The presence of the first-stage product, 3-butene-2-one, is more long-lived than the transient profile demonstrated in Fig. 5(a); persisting for approximately 20 min. 2-Butanone is detected from the onset, reaching a maximum value at *ca.* 19 min and thereafter plateauing in intensity for t > 20 min. Crucially, Fig. 5(b) shows no 2-butanol to be present throughout the full reaction coordinate. Further, the rate of reaction is retarded when compared to that observed for the $Pd(NO_3)_2/Al_2O_3$ catalyst, and the following two statements can be made on the relative magnitude of the associated rate coefficients:

$$k_1 > k_2 \tag{2}$$

and

$$k_3 = 0. \tag{3}$$

The inability of the $PdCl_2/Al_2O_3$ catalyst to participate in the final stage hydrogenation process, *i.e.* 2-butanone → 2-butanol, effectively mimics the pattern previously reported for crotonaldehyde hydrogenation over these catalysts [7]. In a similar manner to that outlined previously [7], reduction of the carbonyl group is thought to be connected with high energy edge sites, that are effectively 'capped' in the case of the $PdCl_2/Al_2O_3$ catalyst due to the presence of residual chloride (Table 1) that is inherently connected with the preparation of that particular catalyst [8]. Infrared spectroscopic investigations of CO chemisorption on both catalysts shows that, unlike the $PdCl_2/Al_2O_3$ catalyst, the metal sites of the $Pd(NO_3)_2/Al_2O_3$ catalyst are unperturbed by chemical residues [8], leaving high energy edge sites available for carbonyl group reduction; in this case facilitating the reduction of a ketone to a secondary alcohol.

Following the lead of the earlier crotonaldehyde hydrogenation study [7], it is proposed that alkyne and alkene reduction takes place at all sites but that carbonyl reduction requires a specific adsorption geometry, which is provided by the edge sites of the Pd nanoparticles. Fig. 6 attempts to illustrate this point schematically. Fig. 6(a) presents a side view of a Pd crystallite where non-specified sites, *e.g.* low index planes, support hydrogenation of 3-butyne-2-one and 3-butene-2-one. Fig. 6(b) proposes that the carbonyl group of the 2-butanone molecule needs to bind to the specified edge site for the subsequent addition of two hydrogen atoms to be achievable. Failure of the 2-butanone to adsorb at this site, for example *via* site blocking by chloride ions, will then prevent this reaction from taking place, as is the case with the $PdCl_2/Al_2O_3$ catalyst (Fig. 5(b) and Eq. (3)).

Please cite this article in press as: C.G.A. Morisse, et al., Structure/activity relationships applied to the hydrogenation of α,β-unsaturated carbonyls: The hydrogenation of 3-butyne-2-one over alumina-supported palladium catalysts, Catal. Today (2016), http://dx.doi.org/10.1016/j.cattod.2016.02.028

The fact that the trends observed for crotonaldehyde hydrogenation over $Pd/Al_2O_3$ are reproduced for 3-butyne-2-one suggest that the proposed structure/activity model [7] may be generically applicable for α,β-unsaturated carbonyl compounds over supported Pd catalysts. The development of models that can reasonably rationalize why certain catalyst formulations favour certain chemical pathways is an important task in catalytic science, and this work indicates how a structural component of a widely utilized heterogeneous catalyst (*i.e.* $Pd/Al_2O_3$) may influence selectivity profiles in stepwise hydrogenation reactions.

Finally, it is noted that the catalysts examined in this work represent an extreme set of structural parameters. Namely, one catalyst possesses accessible edge sites ($Pd(NO_3)_2/Al_2O_3$), whilst these sites are not accessible in the comparison catalyst ($PdCl_2/Al_2O_3$). Whereas it is tempting to suggest that the hydrogenation of α,β-unsaturated carbonyl compounds has the potential to be used as a test reaction to estimate active site distributions for supported Pd catalysts, it is acknowledged that for most supported Pd catalysts the hydrogenation of a carbonyl group under modest conditions of temperature and pressure will not be so quantized, as the catalysts would typically present a distribution of edge sites. Moreover, the relative strength of those adsorption sites might additionally perturb the carbonyl hydrogenation rate and accessibility of particular reaction pathways, *i.e.* selectivity. Nevertheless, the evaluation of the kinetics for the hydrogenation of α,β-unsaturated carbonyl compounds over supported Pd catalysts does possess some potential for estimating the active site distribution of these technologically important materials.

## 4. Conclusions

Transmission infrared spectroscopy has been used to study the gas phase hydrogenation of 3-butyne-2-one over two alumina-supported palladium catalysts in a batch reactor at 373 K. The following conclusions can be drawn.

- The reaction sequence is 3-butyne-2-one → 3-butene-2-one → 2-butanone → 2-butanol over the $Pd(NO_3)_2/Al_2O_3$ catalyst, whereas reaction stops at 2-butanone over a $PdCl_2/Al_2O_3$ catalyst. There is no evidence for a competing sequence where the carbonyl group is initially hydrogenated: 3-butyne-2-one → 3-butyne-2-ol → 3-butene-2-ol → 2-butanol.
- The inability of the $PdCl_2/Al_2O_3$ catalyst to hydrogenate 2-butanone is attributed to chloride residues connected with the catalyst preparative process blocking edge sites, that otherwise would support reduction of the carbonyl functional group.
- Although the adoption of infrared spectroscopy to probe a metal catalysed stepwise hydrogenation process in this case has necessitated a complete vibrational analysis of reagent and product molecules [17], the observation of isosbestic points in the spectra is thought to reflect the presence of equilibria between gaseous and adsorbed phases as well as surface hydrogenation reactions. That information would not normally be accessible in a conventional micro-reactor arrangement sampled by downstream chromatographic methods.
- From comparisons with a previous study on crotonaldehyde hydrogenation, the proposed structure/activity relationship is thought to be generic for the hydrogenation of α,β-unsaturated carbonyl compounds over supported Pd catalysts.

## Acknowledgements

Huntsman Polyurethanes Ltd. and Ineos ChlorVinyls Ltd. are thanked for studentship support (CGAM and ARM respectively). The authors thank the STFC Rutherford Appleton Laboratory for access to neutron beam facilities.

## References

[1] A.T. Bell, Science 299 (2003) 1688–1691.
[2] A.M. Molenbroek, S. Helvig, H. Topsøe, B.S. Clausen, Top. Catal. 52 (2009) 1303–1311.
[3] D.R. Kennedy, G. Webb, S.D. Jackson, D. Lennon, Appl. Catal. A: Gen. 259 (2004) 109–120.
[4] M. Crespo-Quesada, A. Yarulin, M. Jin, Y. Xia, L. Kiwi-Minsker, J. Am. Chem. Soc. 133 (2011) 12787–12794.
[5] A. Yarulin, R.M. Crespo-Quesada, E.V. Egorova, L. Kiwi-Minsker, Kinet. Catal. 53 (2012) 253–261.
[6] A. Presianni, M. Crespo-Quesada, R. Cortese, F. Ferrant, L. Kiwi-Minsker, D. Duca, J. Phys. Chem. C 118 (2014) 3119–3128.
[7] A.R. McInroy, A. Uhl, T. Lear, T.M. Klapötke, S. Shaikhutdinov, S. Schauermann, G. Rupprechter, H.-J. Freund, D. Lennon, J. Chem. Phys. 134 (2011) 214704.
[8] T. Lear, R. Marshall, J.A. Lopez-Sanchez, S.D. Jackson, T.M. Klapötke, G. Rupprechter, M. Bäumer, H.-J. Freund, D. Lennon, J. Chem. Phys. 123 (2005) 174706.
[9] T. Lear, R. Marshall, E.K. Gibson, T. Schütt, T.M. Klapötke, G. Rupprechter, H.-J. Freund, J.M. Winfield, D. Lennon, Phys. Chem. Chem. Phys. 7 (2005) 565–567.
[10] T. Lear, N.G. Hamilton, D. Lennon, Catal. Today 126 (2007) 219–227.
[11] P. Claus, H. Hofmeister, J. Phys. Chem. B 103 (1999) 2766–2775.
[12] M.S. Ide, B. Hao, M. Neurock, R.J. Davis, ACS Catal. 2 (2012) 671–683.
[13] S.D. Jackson, S. Munro, P. Colman, D. Lennon, Langmuir 16 (2000) 6519–6526.
[14] E. Opara, D.T. Lundie, T. Lear, I.W. Sutherland, S.F. Parker, D. Lennon, Phys. Chem. Chem. Phys. 6 (2004) 5588–5595.
[15] A. McFarlane, L. McMillan, I. Silverwood, N.G. Hamilton, D. Siegel, S.F. Parker, D.T. Lundie, D. Lennon, Catal. Today 155 (2010) 206–213.
[16] S.F. Parker, D. Siegel, N.G. Hamilton, J. Kapitán, L. Hecht, D. Lennon, J. Phys. Chem. A 116 (2012) 333–346.
[17] S.F. Parker, I.P. Silverwood, N.G. Hamilton, D. Lennon, Spectrochim. Acta A 153 (2016) 289–297.
[18] G.A. Crowder, Spectrochim. Acta 19A (1963) 1885–1889.
[19] D. Lin-Vien, N.B. Colthup, W.G. Fateley, J.G. Grasselli, The Handbook of Infrared and Raman Characteristic Frequencies of Organic Molecules, Academic Press New York, 1996 (a) p. 131. (b) p. 127. (c) p. 130.
[20] The aldrich library of FT-IR spectra, in: C.J. Pouchert (Ed.), Vapor Phase, vol. 3, ed. 1, Aldrich Chemical Company, Milwaukee, 1985 (a) p. 1595. (b) p. 487.
[21] T. Shimanouchi, Y. Abe, M. Mikami, Spectrochim. Acta 24A (1968) 1037–1058.
[22] M.D. Cohen, E. Fischer, J. Chem. Soc. (1962) 3044–3052.
[23] A.E. Croce, Can. J. Chem. 86 (2008) 918–924.
[24] I.G. Pojarlieff, I.B. Blagoeva, M.M. Toteva, E. Atay, V.T. Angelova, N.G. Vassilev, A.H. Koedjikov, J. Phys. Org. Chem. 21 (2008) 14–22.